ELSEVIER

Volume 454, Issue 1, October 1, 2019

CONTENTS

Abstracted/indexed in: BIOBASE, Biological & Agricultural Index, Biological Abstracts, Biosis Previews, Chemical Abstracts, Current Awareness in Biological Sciences, Current Contents, EMBASE, EMBiology, Genetics Abstracts, MEDLINE®, Science Citation Index. Also covered in the abstract and citation database Scopus. Full text available on ScienceDirect®.

Cover photo. Living colorful Drosophila oocytes.
Different colors of fluorescent protein genes were inserted into the locus of housekeeping gene, ribosomal protein L13A (RPL13A). Every cell in the oocyte has different levels of fluorescent intensities. The fluorescent intensity reflected the expression level of RPL13A from the particular cell. see article by Chen et al., pages 62-69.

0012-1606(20191001)454:1;1-1

Developmental Biology 454 (2019) 66–73

Contents lists available at ScienceDirect

Developmental Biology

journal homepage: www.elsevier.com/locate/developmentalbiology

Parental allele-specific protein expression in single cells *In vivo*

Chiu-An Lo [a], Brian E. Chen [a,b,*]

[a] Centre for Research in Neuroscience, Research Institute of the McGill University Health Centre, Montréal, Québec, Canada
[b] Departments of Medicine and Neurology & Neurosurgery, McGill University, Montréal, Québec, Canada

Quantifying parental allele-specific protein expression over time in single cells in vivo.

A B S T R A C T

Allelic expression from each parent-of-origin is important as a backup and to ensure that enough protein products of a gene are produced. Thus far, it is not known how each cell throughout a tissue differs in parental allele expression at the level of protein synthesis. Here, we measure the expression of the Ribosomal protein L13a (Rpl13a) from both parental alleles simultaneously in single cells in the living animal. We use genome-edited *Drosophila* that have a quantitative reporter of protein synthesis inserted into the endogenous *Rpl13a* locus. We find that individual cells can have large (>10-fold) differences in protein expression between the two parental alleles. Cells can produce protein from only one allele oftentimes, and time-lapse imaging of protein production from each parental allele in each cell showed that the imbalance in expression from one parental allele over the other can invert over time. We also identify the histone methyltransferase EHMT to be involved in the protein synthesis dynamics within cells.

1. Introduction

Protein synthesis is the limiting step in generating the final molecular outcome of DNA. We sought to compare protein expression among different individual cells between tissues, between each parental allele, and over time. However, it has not been possible to measure allele-specific protein expression dynamics in single cells. Thus, in order to track and quantify the dynamics of protein synthesis in single cells in animals, we used the Protein Quantitation Ratioing (PQR) technique (Fig. 1A) (Lo et al., 2015). Using CRISPR-Cas9 genome editing of *Drosophila melanogaster*, we inserted a *PQR* DNA construct with a red fluorescent protein (RFP) reporter at the end of the coding sequence for the *Ribosomal protein L13a* (*Rpl13a*) gene (Lo et al., 2015) (Fig. 1A). This animal produces one molecule of RFP for every one molecule of Rpl13a protein that is made during protein synthesis. Therefore, the red fluorescence intensity in a cell is proportional to the Rpl13a concentration and can be used to track and measure Rpl13a dynamics over time in all optically accessible cells in the animal. We chose Rpl13a because, as a ribosomal subunit, it is itself involved in protein translation and has a long turnover rate similar to fluorescent proteins (Boisvert et al., 2012; Chaudhuri et al., 2007; Jia et al., 2012; Kapasi et al., 2007; Lo et al., 2015; Mazumder et al., 2003). Rpl13a is expressed in all cells at moderately high levels with several hundreds of mRNA copies per cell (Lo et al., 2015). *Rpl13a* mRNA expression dynamics in the brain and in the whole organism are not circadian driven in flies and mice (Hughes et al., 2010, 2012; Keegan et al., 2007). Rpl13a is also frequently used as a control "housekeeping" gene in quantitative DNA measurements because of its resistance to external effects and stability (Mane et al., 2008).

2. Results

2.1. Measuring protein synthesis dynamics in single cells in the awake animal

Inserting *PQR-RFP* into the endogenous *Rpl13a* locus resulted in an entirely red fluorescent animal (Fig. 1B). These *Drosophila* were easily identified by their strong red fluorescence everywhere, which increased globally as the animal developed (Fig. 1B). Although individual cells were not distinguishable in these animals, we used these animals to verify that global Rpl13a is arrhythmic over hourly timescales. To distinguish individual cells, we created two more genome-edited *Drosophila* PQR lines that sequestered RFP or blue fluorescent protein (BFP) into the nucleus, Rpl13a-PQR-RFP_{nols} and Rpl13a-PQR-BFP_{nols} animals, respectively (Fig. 1B). Nuclear localization signals tend to result in fluorescent proteins leaking into the cytosol. We added a nucleolar localization signal (Tsai et al., 2008) to RFP (RFP_{nols}) and BFP (BFP_{nols}) because nucleolar localized fluorescent proteins spread only into the nucleus (Lo et al., 2015).

We tracked endogenous Rpl13a protein production in single cells *in*

* Corresponding author. Centre for Research in Neuroscience, Research Institute of the McGill University Health Centre, Montréal, Québec, Canada.
E-mail address: brian.chen@mcgill.ca (B.E. Chen).

https://doi.org/10.1016/j.ydbio.2019.06.004
Received 2 April 2019; Received in revised form 3 June 2019; Accepted 9 June 2019
Available online 11 June 2019

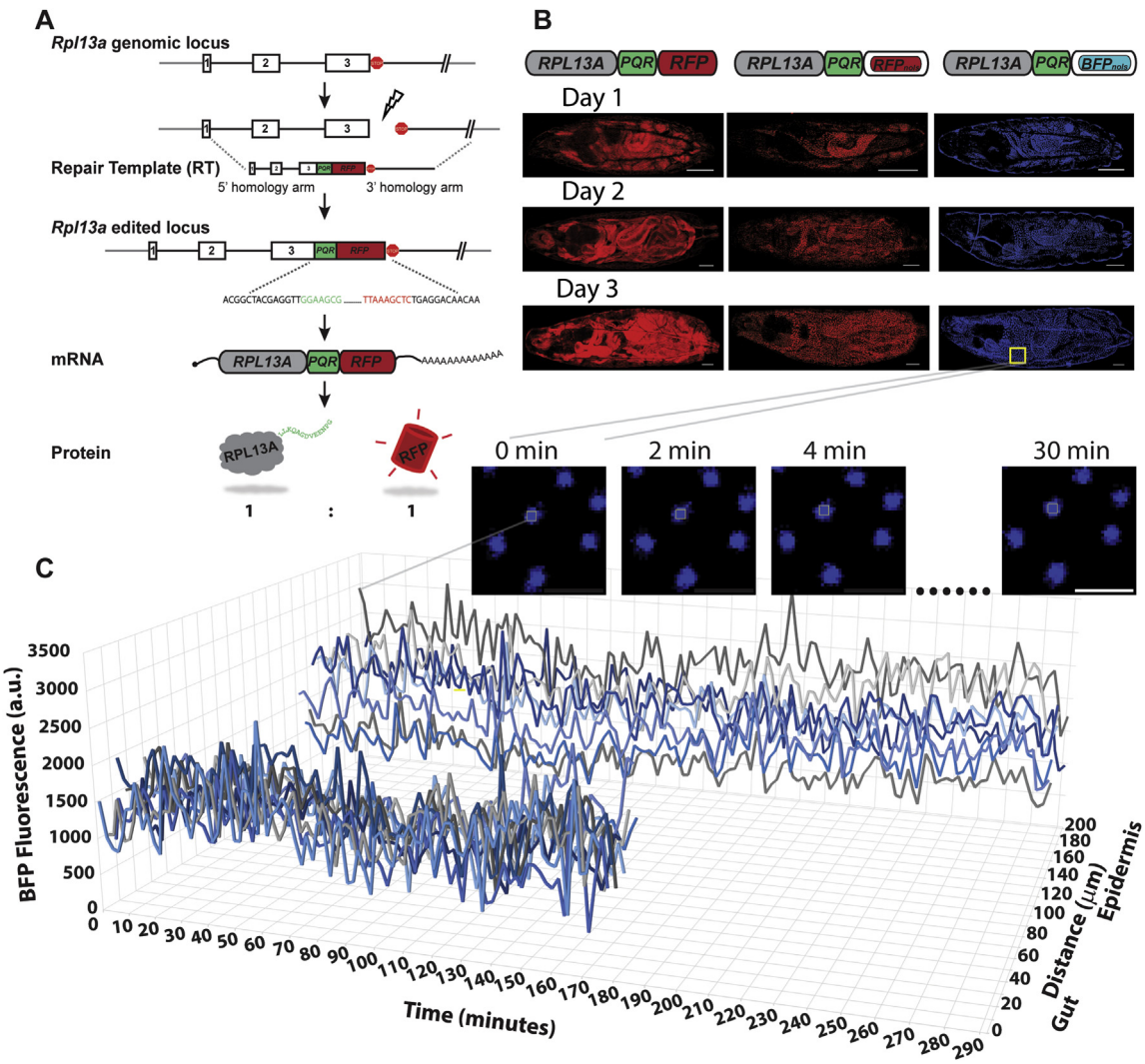

Fig. 1. Quantification of Rpl13a protein production in single cells in the living animal. (A) Insertion of a *Protein Quantitation Reporter* (*PQR*) into the endogenous *Rpl13a* gene can quantify protein amounts. The *PQR* is inserted before the final stop codon using CRISPR-Cas9 genome editing (lightning bolt). The break is repaired using homologous recombination of an exogenous repair template containing the *PQR* and appropriate homology arms. Colored nucleotide sequences represent genomic sequencing results of a *PQR-RFP* insertion into *Drosophila melanogaster*. During protein synthesis the *PQR* produces a stoichiometric ratio of red fluorescent protein (RFP) and Rpl13a protein. (B)Rpl13a increases expression across the larval animal over days. Three different lines of genome-edited *Drosophila melanogaster* were created, Rpl13a-PQR-RFP, Rpl13a-PQR-RFP_{nols} and Rpl13a-PQR-BFP_{nols}. A nucleolar localization signal was used to sequester the RFP or blue fluorescent protein into the nucleus (RFP_{nols} or BFP_{nols}, respectively) to visualize individual cells. Fluorescence intensity in each nucleus is used to measure Rpl13a protein expression. Scale bars, 100 μm (main images), 10 μm (inset). (C)Rpl13a protein expression changes can be measured over hours. Homozygous Rpl13a-PQR-BFP_{nols} larvae were restrained and imaged every 2 min for 5 h. Blue fluorescence intensities from 8 cells in the epidermis and 10 cells from the gut are shown.

vivo by measuring red and blue fluorescence intensities in the nucleus over time scales of seconds to days (**Methods**). To avoid the effects of anesthesia on protein translation, we imaged awake animals immobilized using a suction microfluidics chamber (Mishra et al., 2014). Images were acquired at varying time intervals to verify that the time course of fluorescence signals were not due to changes in animal positioning, movement, imaging depth, photobleaching, or changes in the nucleus and nucleolus (Fig. 1C, **Methods**). At the larval stages after *Drosophila* embryos hatch, mitosis ceases and nearly all cells are fully differentiated and are simply expanding rapidly in size without dividing (Smith and Orr-Weaver, 1991).

2.2. Individual cells can have remarkably imbalanced protein expression for one allele

Mothers produce the oocyte and contribute to it nutrients, proteins, and mRNA molecules, until zygotic expression of both the maternal and paternal genes turn on. We sought to examine the dynamics of protein expression between each of the parent-of-origin *Rpl13a* alleles after zygotic expression turns on. We took advantage of the two colors of the PQR lines and crossed them to create transheterozygous *Rpl13a-PQR-RFP_{nols}/Rpl13a-PQR-BFP_{nols}* animals, from Rpl13a-PQR-RFP_{nols} mothers and Rpl13a-PQR-BFP_{nols} fathers, or vice versa (Fig. 2), to track expression of each allele. We verified that oocytes from Rpl13a-PQR-RFP_{nols} mothers had only red (i.e., maternal expression) within cells (Fig. 2A), until the dark period when all maternal expression is degraded during the maternal to zygotic transition (Baroux et al., 2008; Schier, 2007; Tadros and Lipshitz, 2005). Upon zygotic (i.e., genomic) expression of Rpl13a protein, we found that both parental alleles were expressed at the same time across the organism (Fig. 2A).

What percentage of cells express both the mother's and father's allele at any given time? Imaging transheterozygous larvae at different days, we found that all cells had both red and blue nuclei, as might be expected for a gene expressed at fairly high levels. The majority of cells had similar

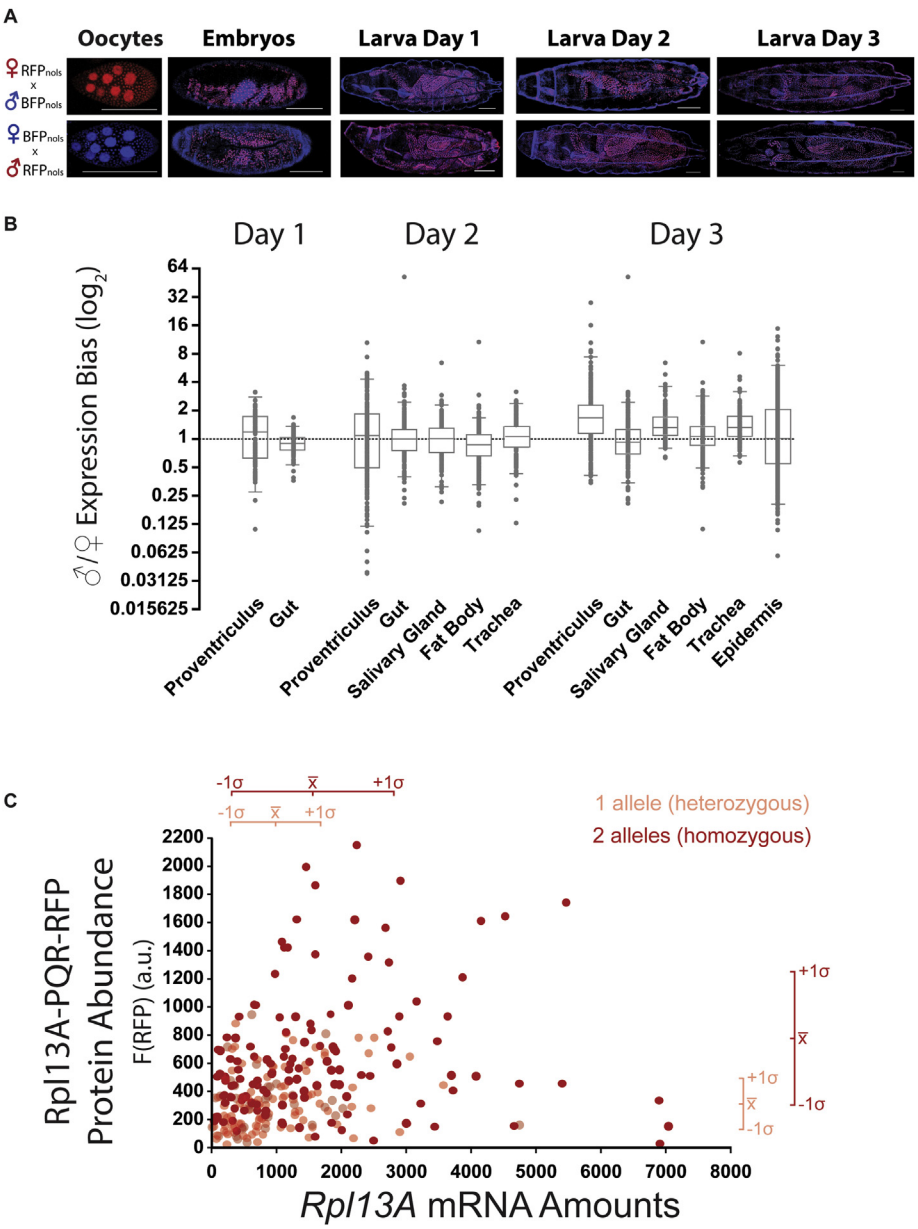

Fig. 2. Large differences between maternal versus paternal allele protein expression can occur in single cells. (A) Rpl13a-PQR-RFP$_{nols}$ and Rpl13a-PQR-BFP$_{nols}$ parents produced transheterozygous progeny whose specific parent-of-origin Rpl13a allele can be tracked using color. Maternal expression of Rpl13a was only detected in oocytes, where it is expressed at high levels and then decreases rapidly in embryos. Rpl13a expression is only detectable again in late embryos, simultaneously from both the maternal and paternal alleles. Most cells express both alleles equally, relative to the blue and red fluorescence intensities, but clusters of cells within the same tissue had similar allelic biases. Scale bars, 100 μm. (B) The ratio of the paternal to maternal Rpl13a protein expression was measured in single cells across different tissues and from both combinations of Rpl13a-PQR-RFP$_{nols}$ and Rpl13a-PQR-BFP$_{nols}$ parents. Box plots represent the median and 1st and 3rd quartiles of the data and whiskers are 2.5 and 97.5 percentiles. (C) The relationships between DNA allele number, RNA, and protein numbers. Single cells were isolated from heterozygous and homozygous Rpl13a-PQR-RFP$_{nols}$ animals and their fluorescence intensities and mRNA amounts were measured. Despite the weak correlation between mRNA and protein levels, the difference between having one copy of DNA expressed versus having two copies of the allele is evident from the population data. Stochastically, homozygous animals are able to reach mRNA and protein levels greater than a single allele is, but mRNA and protein levels from two alleles can often be less than that of a single allele.

fluorescence intensities of RFP and BFP (Fig. 2A). We wanted to know whether there were equivalent levels of mRNA between the parental alleles which might roughly correlate to the similar levels of red and blue fluorescence observed, even though we and others have shown that mRNA amounts correlate poorly with protein quantity, including for *Rpl13a* (Lo et al., 2015; Schwanhausser et al., 2011; Vogel and Marcotte, 2012). We performed qPCR on single cells isolated from trans-heterozygous *Rpl13a-PQR-RFP$_{nols}$/Rpl13a-PQR-BFP$_{nols}$* animals and found 941 ± 1066 mRNA molecules from the maternal allele and 943 ± 878 mRNA molecules from the paternal allele ($n = 53$ cells, 32 animals, 12 from PQR-RFP$_{nols}$ fathers) (Kays and Chen, 2019). These results show that the broadly similar levels of red versus blue fluorescence intensities across the animal do correspond with broadly similar levels of mRNA expression from the respective alleles. We next sought to measure the relative differences between the paternal versus maternal Rpl13a protein expression in individual cells, by adjusting the fluorescence imaging acquisition to be equivalent values between red and blue fluorescence for most cells in the animal. Using the ratio between the red to blue PQR fluorescence expression in each nucleus, we measured the distribution of relative contributions of each parental allele in cells in the proventriculus, gut, salivary gland, fat body, trachea, and epidermis. Most cells expressed both alleles relatively equally, but we frequently observed an imbalance for one parental allele over the other in single cells ($n = 17$ animals, 7 from PQR-RFP$_{nols}$ fathers and 10 from PQR-BFP$_{nols}$ fathers). Occasionally we observed clusters of cells that all had the same imbalanced expression for one allele (Fig. 2A), indicating a clonally inherited initial bias set by early common progenitor cells, but we never observed a complete silencing or systematic bias across the animal for a parental allele (Crowley et al., 2015; DeVeale et al., 2012; Gregg et al., 2010a, 2010b; Wang et al., 2008; Xie et al., 2012). Some cells express very little of one allele leading to differences as large as 64-fold between the two alleles (Fig. 2B). Thus, it is important to note that at the protein level each parental allele in an animal will not necessarily be uniformly expressed in all cells.

Does a heterozygous animal express half as much RNA or protein as a homozygous animal? Our single cell qPCR results show that not every cell transcribes an equal amount of each parental allele, and this is also the case at the protein level, with some cells barely expressing an allele

(Fig. 2B). In other words, if the choice to express either parental allele is stochastic, and the correlation between RNA and protein is poor, then many cells in a heterozygous animal might not necessarily be heterozygous at the RNA nor protein levels. We sought to visualize this relationship between DNA to RNA to protein distributions (Fig. 2C). We isolated 129 single cells from 34 transheterozygous Rpl13a-PQR-RFPnols/Rpl13a-PQR-BFPnols animals and 138 cells from 24 homozygous Rpl13a-PQR-RFPnols animals and then measured their PQR fluorescence intensities before performing single cell qPCR (Kays and Chen, 2019). The linear correlation between *Rpl13a* mRNA and protein expression was weak, with coefficients of determination, R^2 values close to 0. However, the average number of *RFP* mRNA in single cells in the heterozygotes was 979 ± 776 compared to 1650 ± 1241 in the homozygotes. The RFP fluorescence intensity per heterozygous cell was 338 ± 209 compared to 738 ± 484 in the homozygotes. Thus, even with stochastic mechanisms governing the DNA transcription of each allele, RNA expression amounts, and protein synthesis, a large number of cells in an organism averages out the noise to produce more protein from two copies of DNA versus a single copy of the allele.

2.3. Allele-specific imbalances in protein expression change over time

Does a cell maintain its ratio of parental allele expression over time? To measure the protein expression dynamics of both parental alleles, we imaged transheterozygous *Rpl13a-PQR-RFP$_{nols}$/Rpl13a-PQR-BFP$_{nols}$* awake animals every 15 min over time periods of 5 h ($n = 8$ animals, 4 from PQR-RFP$_{nols}$ fathers; Fig. 3A–**C**). Tracking the ratio of expression between the paternal and maternal Rpl13a allele over time from 144 cells revealed that most cells did not show more than a 4-fold bias for either parental allele (Fig. 3D). The average paternal/maternal ratios in single cells over time from different tissues were 1.186 ± 0.858 (epidermis), 1.044 ± 0.709 (salivary gland), and 0.960 ± 0.419 (proventriculus) (mean ± S.D., $n = 5$ animals, 3 from PQR-RFP$_{nols}$ fathers). Thus, over time more than 60% of over 4,400 cells express close to equal amounts between the two parental alleles, but still about 6% of cells will express a $>$ 4-fold difference between the two alleles (Figs. 2B and 3D). Interestingly, this bias can invert, as we found that 21% of cells that expressed a $>$ 2-fold difference between the parental alleles would invert their allele preference ratio to a $>$ 2-fold bias for the other allele (Fig. 3D). This

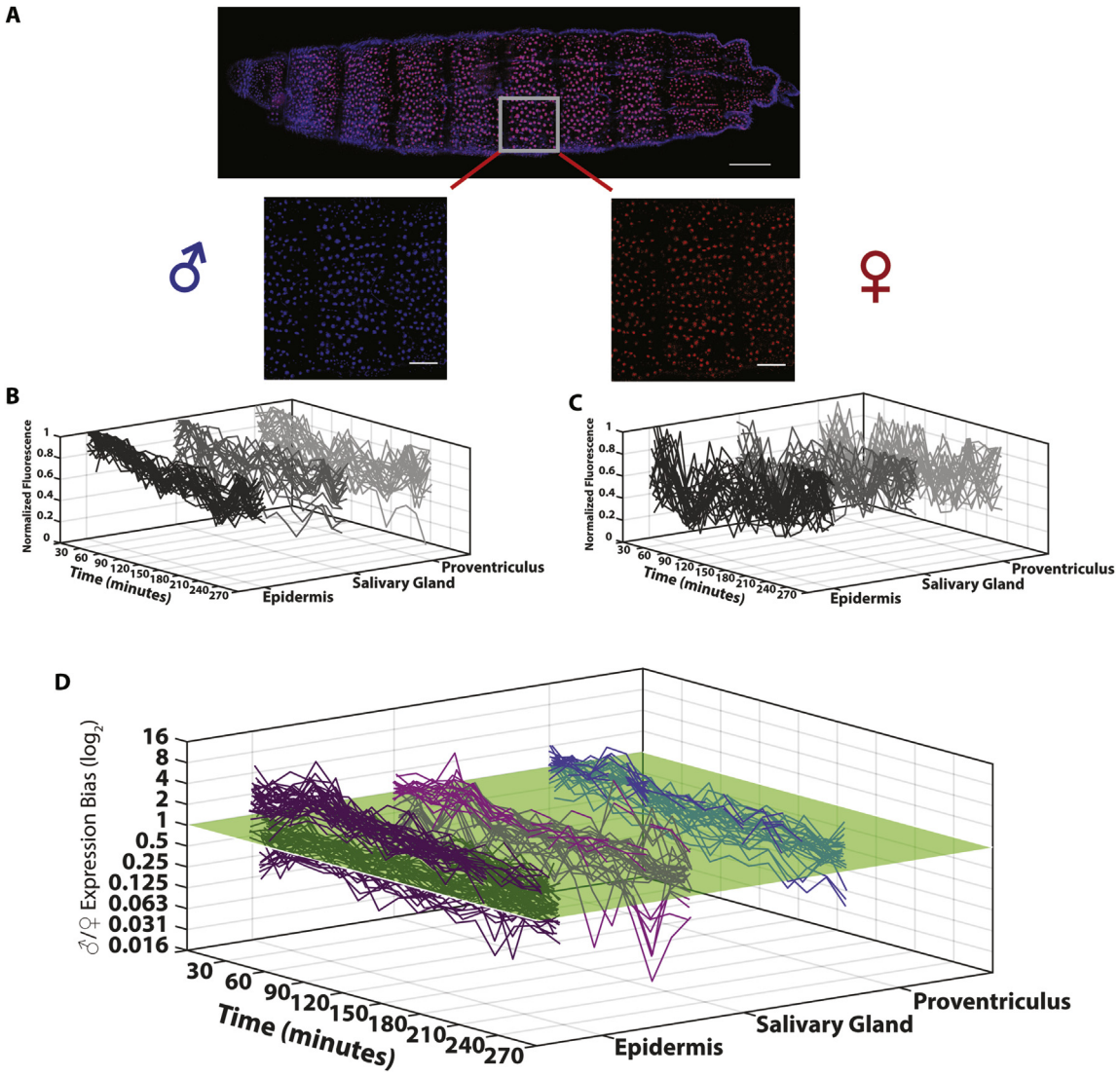

Fig. 3. Parental allele-specific protein expression can change dramatically over time. (A–C) Each parent-of-origin allele of Rpl13a can be tracked and quantified in Rpl13a-PQR-RFP$_{nols}$/Rpl13a-PQR-BFP$_{nols}$ transheterozygous animals using the blue and red fluorescence intensities of the cell nucleus (**A**). Protein synthesis dynamics from paternal (**B**) and maternal (**C**) alleles from each cell in different tissues were measured at 15-min intervals. Scale bars, 100 μm in whole animal image, 50 μm in magnified images. (D) The ratio of paternal to maternal allele expression changes over time. Each curve represents the fluorescence ratio from an individual cell. The surface plane denotes equal expression of paternal and maternal alleles. Curves crossing the surface plane represent an inversion of allele preference expression at the time. The majority of cells maintain close to equal expression of each allele over timescales of hours. However, at any given time many cells will express a $>$ 2-fold expression preference for one parental allele, and even this bias can invert over time.

emphasizes the dynamic nature of allelic expression and shows that the heterozygosity of a single cell can dramatically change over time periods of hours.

2.4. EHMT regulates protein synthesis dynamics

Examining the protein synthesis dynamics of a gene across tissues, cells, and between parental alleles can be used to identify epigenetic regulators of the gene that can control its expression inheritance from progenitor cells, or between parental alleles. However, the expression

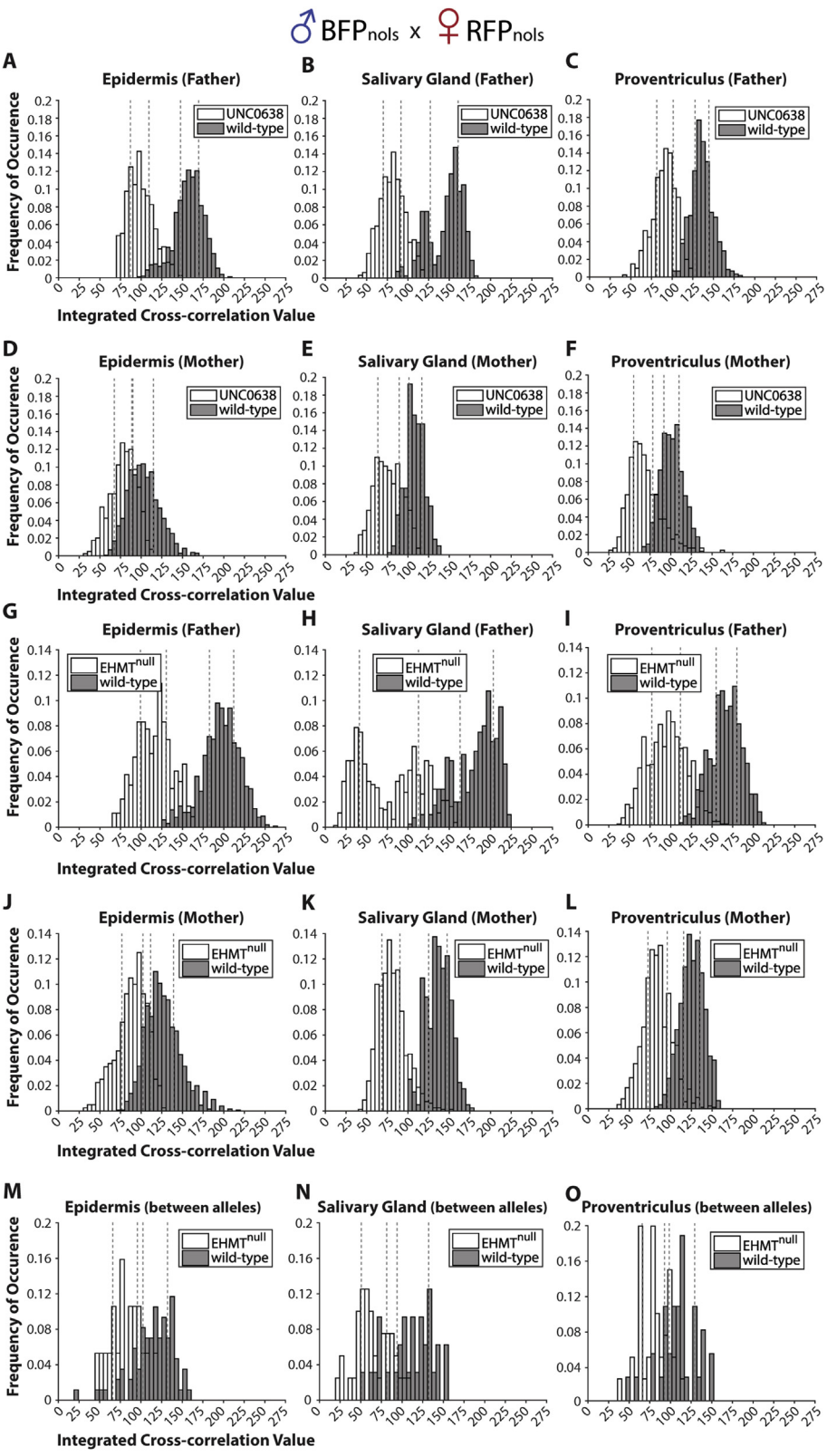

Fig. 4. EHMT regulates protein synthesis dynamics within cells. (A–F) The EHMT enzyme inhibitor UNC0638 decreases the correlation in protein synthesis dynamics between cells within a tissue. (G–L) Loss of function EHMT animals have decreased correlation between cells of their protein synthesis dynamics. (M–O) Loss of function EHMT animals have decreased correlation between parental alleles of their protein synthesis dynamics. Thus, the heritable activity of the EHMT histone methyltransferase regulates the protein synthesis rates across cells and between parental alleles. Dashed grey lines denote 1st and 3rd quartiles in the distribution of integrated cross-correlation values.

dynamics of a highly expressed gene such as *Rpl13a* is likely predominantly stochastic. Thus, we sought to identify histone modifiers that might broadly regulate protein synthesis dynamics across cells. Using specific small-molecule inhibitors of histone lysine methyltransferases, we identified UNC0638 as a potent disruptor of the cross-correlation of Rpl13a protein synthesis dynamics between cells within a tissue (<25% of the cross-correlation values overlap between wild-type and UNC0638-fed animals, Fig. 4A–F). UNC0638 specifically inhibits the histone H3 lysine 9 methyltransferase activity of euchromatic histone-lysine N-methyltransferase (EHMT/GLP). To determine whether EHMT might control *Rpl13a* RNA expression, we performed qPCR on single cells isolated from $EHMT^{null}$ mutants compared to $EHMT^{+}$ control (precise excision). We found that $EHMT^{null}$ mutants had lower levels of *Rpl13a* mRNA (5012 ± 2609, $n = 16$ cells, 2 animals) compared to controls (8463 ± 5524, $n = 17$ cells, 2 animals), indicating that methylation of lysine 9 on histone 3 might coordinate protein synthesis. To verify the specificity of the EHMT histone modification on protein synthesis dynamics, we used two *EHMT* null mutants $EHMT^{DD1}$;; *Rpl13a-PQR-*RFP_{nols}*/Rpl13a-PQR-*BFP_{nols} and $EHMT^{DD2}$;; *Rpl13a-PQR-*RFP_{nols}*/Rpl13a-PQR-*BFP_{nols} (Kramer et al., 2011). We found that loss of function EHMT reduced the cross-correlations of protein synthesis dynamics between cells within the epidermis ($n = 51$ cells, 2 wild-type animals; $n = 19$ cells, 1 *EHMT* null animal), salivary gland ($n = 20$ cells, 1 wild-type animal; $n = 40$ cells, 2 *EHMT* null animals), and proventriculus ($n = 24$ cells, 1 wild-type animal; $n = 65$ cells, 3 *EHMT* null animals), with <25% of the cross-correlation values overlapping between wild-type and *EHMT* null animals (Fig. 4**G–L**). In these same cells, when comparing protein synthesis dynamics between the two alleles, we found that *EHMT* null animals also had lower (<25%) cross-correlations between alleles than wild-type animals (**Fig. 4M–O**), indicating that parental allele expression is regulated independently and that EHMT is involved in this. These results were specific for this histone H3 modification, as the histone H3 lysine 27 demethylase mutant *UTX* (Copur and Muller, 2013) had a broad overlap of cross-correlation values compared to wild-type (Supplemental Fig. S1). These results demonstrate that EHMT alters ribosomal gene expression dynamics to control protein synthesis rates. Histone methylation may be one mechanism by which ribosomal availability can be regulated and specific parental allele expression can be controlled.

3. Discussion

We used fluorescent proteins to report the protein expression of Rpl13a. After protein synthesis of Rpl13a and the PQR fluorescent protein reporter, both proteins must fold and mature to function. It is not known how long the Rpl13a protein takes to function after its synthesis, but it is similar in size to the red and blue fluorescent proteins used in our experiments, which we estimate to take 1 h to fluoresce after synthesis at 25 °C (Balleza et al., 2018). Therefore, we analyzed the ratios of fluorescence intensities between cells and between alleles rather than quantifying amounts of functional Rpl13a.

Although protein activity is the ultimate executor of gene expression, RNA levels are frequently used as a proxy, and so knowing the correlation between a gene's mRNA and protein products is important to many biologists. For example, up to half of proteins with circadian rhythms do not have rhythmic mRNAs (Reddy et al., 2006; Robles et al., 2014). Protein abundance is critically important in some genes, where the loss of expression of one copy of the gene can cause diseases and disorders collectively called haploinsufficiencies. Previous studies have demonstrated within single cells the random monoallelic expression of some genes, so that at any given moment only one copy is expressed. This means that depending on the gene, cells from a homozygous animal might not express twice as many mRNA molecules as those from a heterozygous (Deng et al., 2014; Gimelbrant et al., 2007; Levesque et al., 2013). This has important consequences in disease. For example, random X-inactivation of the *MECP2* gene results in monoallelic expression; but, in the case of a mutant *MECP2* gene in Rett syndrome this leads to a random mixed population of normal MECP2 neurons interconnected with dysfunctional MECP2 neurons within the brain.

Our results examining allelic expression at the RNA and protein levels demonstrate that heterozygous and homozygous definitions vary from cell to cell and over time. For example, this asymmetry could allow one parental allele with a disease mutation to be the one solely expressed during transcription, or spatially during local translation in a neuron's dendrite. Sections of dendrites with reduced or improper function across multiple neural circuits in a brain may be the difficult molecular reality underlying a number of neurological disorders. This would be a more fine-scale version of the disease-gene random monoallelic expression example described above.

Overall within a tissue, the protein expression between two alleles balances out (Fig. 2B), but still, close to 50% of cells in an animal can have a > 2-fold difference between the two alleles. Furthermore, these biases can change over time in single cells (Fig. 3D), further highlighting the fluid definition of allelic expression. Despite the noise in mRNA and protein production, the underlying structure that is set by the integer copy numbers of DNA (i.e., one allele expression versus two allele expression) is clear and detectable with even a moderate number of cells (Fig. 2C). These cellular and temporal differences in allelic expression have important consequences for understanding diseases caused by haploinsufficiency and copy number variations. Our study demonstrates a new paradigm to examine parental allele-specific expression at the protein level in single cells over time in the living animal. This new approach can be useful in examining genes subject to imprinting where only a specific parent-of-origin allele is expressed due to the presence of inherited epigenetic controllers. Tracking the inheritance of epigenetic signatures that control allelic expression across multiple cell divisions of individual cells can be performed in real time *in vivo*.

4. Experimental procedures

4.1. Preparation of sgRNA expression vectors

Different single guide RNAs (sgRNAs) were designed in a 20 base pair DNA oligonucleotide format to guide the Cas9 nuclease to the end of the coding region of *Drosophila Rpl13a*. They were optimized using the online Optimal Target Finder algorithm (http://tools.flycrispr.molbio.wisc.edu/targetFinder). Individual sgRNAs were synthesized and cloned into the backbone of the *pCFD3: U6:*3-gRNA vector (Addgene #49410) (Port et al., 2014). Each sgRNAs was co-transfected along with a Cas9 expressing plasmid, pBS-Hsp70-Cas9 (Addgene #46294), and a circular *Rpl13a* repair template into cultured *Drosophila S2* cells using TransIT Insect Transfection Reagent (Mirus Bio LLC, Madison, WI, USA). Gene editing efficiency of the different sgRNAs was evaluated five days after transfection by cellular fluorescence and genotyping using a primer outside of the homology arm and the other inside the inserted *PQR* sequence.

4.2. Construction of PQR repair template

The genomic sequences of *Drosophila Ribosomal protein L13A* were identified using GeneDig (https://genedig.org) (Suciu et al., 2015) and then PCR amplified from Canton-S fly genomic DNA lysates to construct the 5′ and 3′ homology arms of 1.4 kilobase each. The 5′ homology arm did not include the endogenous *Rpl13a* promoter, to prevent the expression of the transgene until the in-frame genomic integration at the correct locus. The three different *Protein Quantitation Reporters* with a fluorescent protein with and without a nucleolar localization signal were inserted between the 5′ and 3’ homology arms to generate three different *Rpl13a*-specific repair templates as described (Lo et al., 2015).

4.3. Generation of sgRNA-expressing transgenic fly

The optimal sgRNA in *pCFD3: U6:*3-gRNA vector was microinjected

into embryos (BestGene, Inc) to create a transgenic fly constitutively expressing the *Rpl13a*-specific sgRNA. This sgRNA fly was then crossed to a *nos-Cas9* fly (*yw*; *attP40 {nos-Cas9}/CyO*) to restrict CRISPR-Cas9 activity to minimize lethality (Port et al., 2014). Circular *Rpl13a* repair template was then microinjected into the embryos containing both active Cas9 and sgRNA (BestGene, Inc). Surviving flies were intercrossed with one another and the resulting offspring were screened for red or blue fluorescence signals at wandering 3rd instar larval stage. RFP or BFP positive larvae were collected and out-crossed to the Canton-S strain to remove the Cas9 and sgRNA genes. The integrated *PQR-RFP*, *PQR-RFP$_{nols}$*, or *PQR-BFP$_{nols}$* at the *Rpl13a* locus at the 3rd chromosome was balanced by crossing to a TM3 balancer line. All three of the genome-edited fly lines (Rpl13a-PQR-RFP, Rpl13a-PQR-RFP$_{nols}$ and Rpl13a-PQR-BFP$_{nols}$) were verified by genotyping and sequencing.

4.4. Fly husbandry

Flies of different genotypes were reared in a 25 °C humidity-controlled incubator with a 12:12 h light/dark cycle. Embryos were collected for 4 h (stage 12–16) on apple juice agar plates and the hatched larvae were imaged at the next day or 2 or 3 days later. Homozygous and transheterozygous embryos or larvae were collected for imaging. Oocytes from transheterozygous females were used to confirm maternal expression of Rpl13a, which was expressed strongly, but then decreased rapidly in embryos.

EHMT null (*EHMT^{DD1}*;; *Rpl13a-PQR-RFP$_{nols}$/Rpl13a-PQR-BFP$_{nols}$* and *EHMT^{DD2}*; ; *Rpl13a-PQR-RFP$_{nols}$/Rpl13a-PQR-BFP$_{nols}$*) larvae were obtained by crossing *w;; Rpl13a-PQR-RFP$_{nols}$/TM3* to *EHMT^{null}* imprecise p-element excision flies (gifts from Dr. Annette Schenck). The control EHMT fly line used was the precise excision of the same genetic background (Kramer et al., 2011). Larvae were used at 3 days old for experiments. UNC0638 containing apple agar plates were used to collect embryos and used for the larvae food source. These larvae were used at 3 days old for experiments.

4.5. Quantitative real-time PCR

Single cell imaging and subsequent qPCR was performed as previously described (Kays and Chen, 2019; Lo et al., 2015). Individual cells were imaged in drops of culture media on Teflon-coated glass slides before extraction and purification of total RNA using the TRIzol reagent (Life Technologies). Total RNA was reverse-transcribed with gene-specific primers (2 μM final concentration) using Superscript III reverse-polymerase (Life Technologies). This cDNA template was used for real-time PCR using the TaqMan Fast Advanced Mastermix (Life Technologies). Real-time PCR amplification was detected using the StepOnePlus Real-Time PCR System (Applied Biosystems) and cycle quantification values were calculated using the StepOne software. Experiments were performed in two to three experimental replicates with two technical replicates. Absolute quantification was determined using standard curves generated with synthesized oligo standards containing the *Rpl13a* target. Primers specific for *Rpl13a-PQR-RFP* and *Rpl13a-PQR-BFP* were less efficient (86%) than primers for wildtype *Rpl13a*, which can result in less accurate absolute RNA quantifications. Primers and double-quenched 5′-FAM/ZEN/IowaBlackFQ-3′ probes were purchased from Integrated DNA Technologies (Coralville, IA).

4.6. Image acquisition

Fluorescence images were taken using an Olympus laser scanning confocal microscope FV1000 at 800 × 800 pixels with a 20 × or 40 × oil objective, N.A. 0.85 and 1.30 corresponding to a 636 × 636 μm and 317 × 317 μm field of view, respectively, or a custom built 2-photon laser scanning microscope at 512 × 512 pixels with a 40 × water objective, 1.0 N.A. corresponding to an approximately 310 × 310 μm field of view. Fluorescence emission was detected by photomultiplier tubes. All image acquisition parameters were fixed during imaging sessions for excitation intensity, exposure time, gain, and voltages. Animals were imaged at late stage embryos (>16 h after egg laying), and three different developmental stages (1, 2, and 3 days after hatching) of the transparent larvae. For long term time-lapse imaging, larvae were immobilized and accommodated in a microfluidic chamber (larva chip) over the course of imaging (Mishra et al., 2014). Larvae were coated with Halocarbon 700 oil to avoid dehydration. Images were acquired between every 60 s, 2, 4, 5, or 15 min for 3–7 h total duration to verify that the time constant for fluorescence changes (see below) were not due to animal positioning, movement, imaging depth, or photobleaching, regardless of sampling frequency.

4.7. Image analysis

Average fluorescence pixel intensities were measured in one region of interest (of 2 × 2, 4 × 4, or 5 × 5 pixels for epidermal, fat body, or gut cells, respectively) that covered 70% of the nuclei using ImageJ as described (Lo et al., 2015). Fluorescence pixel intensities were background subtracted and presented in arbitrary units. No bleed-through was detected between red and blue fluorescence channels. Images in figures were adjusted for contrast and brightness for presentation. To verify that changes in fluorescence intensity over time were not due to changes in nucleolar and nucleus size and shape, we imaged Rpl13a-PQR-RFP animals where the RFP fluorescence is within the cytosol (Fig. 1B). In initial experiments we crossed Rpl13a-PQR-RFP with Rpl13a-PQR-BFP$_{nols}$ animals to use the blue nucleus as a marker for individual cells, but the RFP was found to dimerize with the BFP and accumulate in the nucleus, as we have observed previously in mammalian cells. In Rpl13a-PQR-RFP animals, we analyzed cytoplasmic RFP fluorescence dynamics in putative single cells using one region of interest of 6 × 6 pixels. The fluorescence dynamics were not significantly different from animals with fluorescence contained within the nucleus, with an average time constant of $\tau = 8.3 \pm 7.8$ min from cytoplasmic fluorescence (mean ± S.D., $n = 36$ cells, 3 animals) compared to 8.5 ± 8.1 min from the nuclear fluorescence.

4.8. Statistical analysis

All statistical analyses and cross-correlation analyses were performed using custom-written programs in MatLab (MathWorks, Natick, MA). We simulated stochastic RNA and protein expression from two alleles in 10, 100, and 1,000 cells to examine their distributions of expression, which were in agreement with our experimental data obtained (Fig. 2C). These RNA and protein simulations comparing heterozygous and homozygous alleles were performed using custom-written programs (available on request) in MatLab.

Acknowledgments

The authors thank Ibrahim Kays, Farida Emran, Júnia Vieira dos Santos, Isabela Fabri Karam, Leah Dawson, and ChenHui Zhao for assistance with experiments and analysis. This work was supported by grants (to B.E.C.) from the Natural Sciences and Engineering Research Council of Canada (386341), and the Canadian Institutes of Health Research (148882).

Appendix A. Supplementary data

Supplementary data to this article can be found online at https://doi.org/10.1016/j.ydbio.2019.06.004.

Author contributions

B.E.C. designed the experiments and supervised the project. C.L. and B.E.C. performed experiments and analyzed the data. C.L. and B.E.C. wrote the manuscript.

No competing financial interests to declare.

References

Balleza, E., Kim, J.M., Cluzel, P., 2018. Systematic characterization of maturation time of fluorescent proteins in living cells. Nat. Methods 15, 47–51.

Baroux, C., Autran, D., Gillmor, C.S., Grimanelli, D., Grossniklaus, U., 2008. The maternal to zygotic transition in animals and plants. Cold Spring Harbor Symp. Quant. Biol. 73, 89–100.

Boisvert, F.M., Ahmad, Y., Gierlinski, M., Charriere, F., Lamont, D., Scott, M., Barton, G., Lamond, A.I., 2012. A quantitative spatial proteomics analysis of proteome turnover in human cells. Mol. Cell. Proteom. 11. M111 011429.

Chaudhuri, S., Vyas, K., Kapasi, P., Komar, A.A., Dinman, J.D., Barik, S., Mazumder, B., 2007. Human ribosomal protein L13a is dispensable for canonical ribosome function but indispensable for efficient rRNA methylation. RNA 13, 2224–2237.

Copur, O., Muller, J., 2013. The histone H3-K27 demethylase Utx regulates HOX gene expression in Drosophila in a temporally restricted manner. Development 140, 3478–3485.

Crowley, J.J., Zhabotynsky, V., Sun, W., Huang, S., Pakatci, I.K., Kim, Y., Wang, J.R., Morgan, A.P., Calaway, J.D., Aylor, D.L., Yun, Z., Bell, T.A., Buus, R.J., Calaway, M.E., Didion, J.P., Gooch, T.J., Hansen, S.D., Robinson, N.N., Shaw, G.D., Spence, J.S., Quackenbush, C.R., Barrick, C.J., Nonneman, R.J., Kim, K., Xenakis, J., Xie, Y., Valdar, W., Lenarcic, A.B., Wang, W., Welsh, C.E., Fu, C.P., Zhang, Z., Holt, J., Guo, Z., Threadgill, D.W., Tarantino, L.M., Miller, D.R., Zou, F., McMillan, L., Sullivan, P.F., Pardo-Manuel de Villena, F., 2015. Analyses of allele-specific gene expression in highly divergent mouse crosses identifies pervasive allelic imbalance. Nat. Genet. 47, 353–360.

Deng, Q., Ramskold, D., Reinius, B., Sandberg, R., 2014. Single-cell RNA-seq reveals dynamic, random monoallelic gene expression in mammalian cells. Science 343, 193–196.

DeVeale, B., van der Kooy, D., Babak, T., 2012. Critical evaluation of imprinted gene expression by RNA-Seq: a new perspective. PLoS Genet. 8, e1002600.

Gimelbrant, A., Hutchinson, J.N., Thompson, B.R., Chess, A., 2007. Widespread monoallelic expression on human autosomes. Science 318, 1136–1140.

Gregg, C., Zhang, J., Butler, J.E., Haig, D., Dulac, C., 2010a. Sex-specific parent-of-origin allelic expression in the mouse brain. Science 329, 682–685.

Gregg, C., Zhang, J., Weissbourd, B., Luo, S., Schroth, G.P., Haig, D., Dulac, C., 2010b. High-resolution analysis of parent-of-origin allelic expression in the mouse brain. Science 329, 643–648.

Hughes, M.E., Grant, G.R., Paquin, C., Qian, J., Nitabach, M.N., 2012. Deep sequencing the circadian and diurnal transcriptome of Drosophila brain. Genome Res. 22, 1266–1281.

Hughes, M.E., Hogenesch, J.B., Kornacker, K., 2010. JTK_CYCLE: an efficient nonparametric algorithm for detecting rhythmic components in genome-scale data sets. J. Biol. Rhythm. 25, 372–380.

Jia, J., Arif, A., Willard, B., Smith, J.D., Stuehr, D.J., Hazen, S.L., Fox, P.L., 2012. Protection of extraribosomal RPL13a by GAPDH and dysregulation by S-nitrosylation. Mol. Cell 47, 656–663.

Kapasi, P., Chaudhuri, S., Vyas, K., Baus, D., Komar, A.A., Fox, P.L., Merrick, W.C., Mazumder, B., 2007. L13a blocks 48S assembly: role of a general initiation factor in mRNA-specific translational control. Mol. Cell 25, 113–126.

Kays, I., Chen, B.E., 2019. Protein and RNA quantification of multiple genes in single cells. Biotechniques 66, 15–21.

Keegan, K.P., Pradhan, S., Wang, J.P., Allada, R., 2007. Meta-analysis of Drosophila circadian microarray studies identifies a novel set of rhythmically expressed genes. PLoS Comput. Biol. 3, e208.

Kramer, J.M., Kochinke, K., Oortveld, M.A., Marks, H., Kramer, D., de Jong, E.K., Asztalos, Z., Westwood, J.T., Stunnenberg, H.G., Sokolowski, M.B., Keleman, K., Zhou, H., van Bokhoven, H., Schenck, A., 2011. Epigenetic regulation of learning and memory by Drosophila EHMT/G9a. PLoS Biol. 9, e1000569.

Levesque, M.J., Ginart, P., Wei, Y., Raj, A., 2013. Visualizing SNVs to quantify allele-specific expression in single cells. Nat. Methods 10, 865–867.

Lo, C.-A., Kays, I., Emran, F., Lin, T.-J., Cvetkovska, V., Chen, Brian E., 2015. Quantification of protein levels in single living cells. Cell Rep. 13, 2634–2644.

Mane, V.P., Heuer, M.A., Hillyer, P., Navarro, M.B., Rabin, R.L., 2008. Systematic method for determining an ideal housekeeping gene for real-time PCR analysis. J. Biomol. Tech. : J. Biochem. (Tokyo) 19, 342–347.

Mazumder, B., Sampath, P., Seshadri, V., Maitra, R.K., DiCorleto, P.E., Fox, P.L., 2003. Regulated release of L13a from the 60S ribosomal subunit as a mechanism of transcript-specific translational control. Cell 115, 187–198.

Mishra, B., Ghannad-Rezaie, M., Li, J., Wang, X., Hao, Y., Ye, B., Chronis, N., Collins, C.A., 2014. Using microfluidics chips for live imaging and study of injury responses in Drosophila larvae. J. Vis. Exp., e50998

Port, F., Chen, H.M., Lee, T., Bullock, S.L., 2014. Optimized CRISPR/Cas tools for efficient germline and somatic genome engineering in Drosophila. Proc. Natl. Acad. Sci. U.S.A. 111, E2967–E2976.

Reddy, A.B., Karp, N.A., Maywood, E.S., Sage, E.A., Deery, M., O'Neill, J.S., Wong, G.K., Chesham, J., Odell, M., Lilley, K.S., Kyriacou, C.P., Hastings, M.H., 2006. Circadian orchestration of the hepatic proteome. Curr. Biol. 16, 1107–1115.

Robles, M.S., Cox, J., Mann, M., 2014. In-vivo quantitative proteomics reveals a key contribution of post-transcriptional mechanisms to the circadian regulation of liver metabolism. PLoS Genet. 10, e1004047.

Schier, A.F., 2007. The maternal-zygotic transition: death and birth of RNAs. Science 316, 406–407.

Schwanhausser, B., Busse, D., Li, N., Dittmar, G., Schuchhardt, J., Wolf, J., Chen, W., Selbach, M., 2011. Global quantification of mammalian gene expression control. Nature 473, 337–342.

Smith, A.V., Orr-Weaver, T.L., 1991. The regulation of the cell cycle during Drosophila embryogenesis: the transition to polyteny. Development 112, 997–1008.

Suciu, R.M., Aydin, E., Chen, B.E., 2015. GeneDig: a web application for accessing genomic and bioinformatics knowledge. BMC Bioinf. 16, 67.

Tadros, W., Lipshitz, H.D., 2005. Setting the stage for development: mRNA translation and stability during oocyte maturation and egg activation in Drosophila. Dev. Dynam. 232, 593–608.

Tsai, K.W., Tseng, H.C., Lin, W.C., 2008. Two wobble-splicing events affect ING4 protein subnuclear localization and degradation. Exp. Cell Res. 314, 3130–3141.

Vogel, C., Marcotte, E.M., 2012. Insights into the regulation of protein abundance from proteomic and transcriptomic analyses. Nat. Rev. Genet. 13, 227–232.

Wang, X., Sun, Q., McGrath, S.D., Mardis, E.R., Soloway, P.D., Clark, A.G., 2008. Transcriptome-wide identification of novel imprinted genes in neonatal mouse brain. PLoS One 3, e3839.

Xie, W., Barr, C.L., Kim, A., Yue, F., Lee, A.Y., Eubanks, J., Dempster, E.L., Ren, B., 2012. Base-resolution analyses of sequence and parent-of-origin dependent DNA methylation in the mouse genome. Cell 148, 816–831.